Electronic Supplementary Information (ESI)

Mononuclear indium(III) photosensitizers for photo-dehalogenation and olefin reduction

Li-Zhi Fu,[a] Piao He,[a] Jia-Wei Wang,[b] Fan Ma,[a] Chao Liu,[a] Guo Chen,[a] Xiao-Yi Yi*[a]

[a] College of Chemistry and Chemical Engineering, Central South University, Changsha, Hunan 410083, P. R. China

[b] School of Chemical Engineering and Technology, Sun Yat-sen University, Zhuhai 519082, China

Email: xyyi@csu.edu.cn

Phone: 86-731-88879616

Contents

1. General Conidiations

1.1 Materials

All syntheses were carried using a standard vacuum line and Schlenk technology with an atmosphere of purified argon. Solvents for air- and moisture-sensitive manipulations were dried and deoxygenated using a JC-Meyer Phoenix solvent drying system. The ligands **HL1** (2-(1Hpyrrol-2-yl)pyridine), **HL2** (2-(4-methyl-1H-pyrrol-2-yl)pyridine), **HL3** (2-(3,5-dimethyl-1H-pyrrol-2-yl)pyridine), and **HL4** (2-(3,4,5-trimethyl-1H-pyrrol-2-yl)pyridine) were prepared according to literature methods.[1, 2] All other chemicals were obtained from J&K Scientific Ltd and used without further purification.

1.2 Characterization

The ^{1}H NMR spectra were recorded on a Bruker AVANCE (III) 400M spectrometer. The infrared spectra (in KBr) were recorded on a Nicolet 6700 spectrometer FT-IR spectrophotometer. The UV-Vis spectra were recorded on an Agilent Technologies Cary 8454 UV-Vis spectrometer at ambient temperature with a 1 cm quartz cell. ESI-MS was performed on a Bruker Daltonik GmbH, Bremen mass spectrometer equipped with an electrospray ionization (ESI) source. Emission spectra were recorded on a F97Pro Fluorescence spectrometer. The quantum yields were carried out on a fluorescence spectrometer (F-7000, Hitachi, Japan) equipped with an integrating sphere, which was also reproduced on fluorescence spectrometer (FLS 1000, Edinburgh Instruments LTD.). The excited-state lifetimes (τ) were conducted on a modular fluorescent life and steady-state fluorescence spectrometer (FLS 1000, Edinburgh Instruments LTD.). The photocatalytic reaction experiments are performed by the Perfect Light PCX50C photochemistry system. Cyclic voltammetry was performed on a CHI Instruments CHI660e electrochemical analyzer. The working electrode was a glassy carbon electrode, the counter electrode is a Pt wire, and the reference electrode is an Ag/AgCl electrode in saturated KCl. Electrochemical measurements were performed in acetonitrile solution containing 0.1 M $tBu_4N{\cdot}PF_6$ electrolyte in a one compartment cell. All potentials were converted to $E_{1/2}$ vs. $Cp_2Fe^{+/0}$ in CH_3CN by adding -0.43 V to the measured potential.

X-ray Diffraction Studies: Diffraction data was record on a Bruker CCD diffractometer with monochromatized Mo-Kα radiation (λ= 0.71073 Å). The collected frames are processed using the software SAINT. The absorption correction was processed with SADABS. The structure was solved by a direct method and refined using a full matrix least squares method on F^2 with the SHELXTL software package. Atomic positions of non-hydrogen atoms were refined with anisotropic parameters. All hydrogen atoms were introduced at their geometrical positions and refined as riding atoms.

DFT calculations were performed by using the Gaussian 09 package. Geometry optimizations were performed on the ground state structures with the Becke's three-parameter B3LYP exchange-correlation functional.The all-electron Gaussian basis

sets were those developed by the Ahlrichs group. The slightly smaller polarized split-valence def2-SVP basis sets for H, C, N and triple-ζ quality basis sets def2-TZVP with one set of polarization functions for the In atom. Vibrational frequencies were calculated based on the optimized structures to confirm the absence of imaginary frequencies. MOs of complexes were calculated and visualized as well. The excited states calculations were carried out on the basis of the optimized S0 structures via time-dependent DFT (TD-DFT) at the same level. The solvation effects were also taken into account using the self-consistent reaction field (SCRF) and a universal solvation model density (SMD) with the CH_3CN solvent.

2. Experimental Procedures and Spectroscopic Data

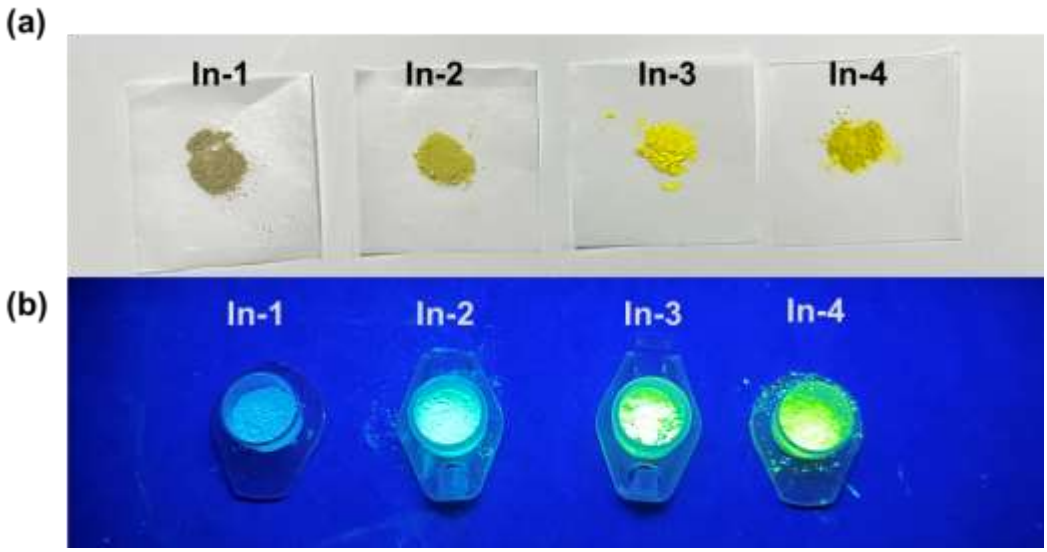

Figure S1. (a) solid samples of **In-1** – **In-4**; (b) solid samples of **In-1** – **In-4** upon irradiation at 365 nm at room temperature.

Synthesis of In-1: $InMe_3$ (48.0 mg, 0.3 mmol) was slowly added to the solution of **HL1** (140.0 mg, 1.0 mmol) in toluene (5 mL). The reaction mixture was stirred for 2 hours at room temperature then heated to reflux overnight under nitrogen atmosphere to give a green solution. After cooling, toluene was removed in vacuo. The solid residue was washed three times with diethyl ether to remove any unreacted **HL1**. The crude product was redissolved in CH_2Cl_2 and filtered. Recrystallized by the addition of diethyl ether to give the desired product **In-1** as a grey green solid. Yield: 101 mg (62%). The solution of **In-1** in CH_2Cl_2 was layered by hexane to give block single crystals which were suitable for X-ray diffraction analysis.

^{1}H NMR (400 MHz, $CDCl_3$) δ 8.33 (d, J = 5.0 Hz, 1H), 7.77 – 7.70 (m, 1H), 7.64 (d, J = 8.2 Hz, 1H), 7.16 – 7.06 (m, 1H), 6.88 (dd, J = 3.4, 1.0 Hz, 1H), 6.73 (dd, J = 1.7, 1.1 Hz, 1H), 6.30 (dd, J = 3.3, 2.0 Hz, 1H).

ESI-MS (m/z): 567.1044, calcd. 567.0759 for $[M + K^+]^+$.

IR (KBr, cm^{-1}): 1604 (s), 1525 (s), 1444 (s), 1390 (m), 1274 (m), 1159 (m), 1051 (m), 1000 (m), 944 (s), 728 (s), 518 (w).

Synthesis of In-2: $InMe_3$ (80.0 mg, 0.5 mmol) was slowly added to the solution of **HL2** (260.0 mg, 1.65 mmol) in toluene (5 mL). The reaction mixture was stirred for 2 hours at room temperature then heated to reflux overnight under nitrogen atmosphere to give a dark-green solution. After cooling, toluene was removed in vacuo. The solid residue was washed three times with diethyl ether to remove any unreacted **HL2**. The crude product was redissolved in CH_2Cl_2 and filtered. Recrystallized by the addition of diethyl ether to give the desired product **In-2** as a yellow solid. Yield: 152.4 mg (52%).

^{1}H NMR (400 MHz, $CDCl_3$) δ 7.58 (dd, J = 14.8, 6.6 Hz, 2H), 7.48 (d, J = 8.2 Hz, 1H), 6.81 (t, J = 6.1 Hz, 1H), 6.67 (s, 1H), 6.48 (s, 1H), 2.20 – 2.06 (m, 3H).

ESI-MS (m/z): 585.0781, calcd. 585.1252 for $[M]^+$.

IR (KBr, cm^{-1}): 2919 (w), 2963 (w), 1601 (s), 1542 (m), 1439 (s), 1361 (m), 1288 (w), 1153 (w), 1105 (w), 964 (s), 769 (w), 615 (w), 489 (w).

Synthesis of In-3: $InMe_3$ (95.94 mg, 0.6 mmol) was slowly added to the solution of **HL3** (292.6 mg, 1.7 mmol) in toluene (5 mL). The reaction mixture was stirred for 2 hours at room temperature then heated to reflux overnight under nitrogen atmosphere to give a yellow solution. After cooling, toluene was removed in vacuo. The solid residue was washed three times with diethyl ether to remove any unreacted **HL3**. The crude product was redissolved in CH_2Cl_2 and filtered. Recrystallized by the addition of diethyl ether to give the desired product **In-3** as a light-yellow solid. Yield: 263.8 mg (70%). The solution of **In-3** in CH_2Cl_2 was layered by hexane to give block yellow single crystals which were suitable for X-ray diffraction analysis.

^{1}H NMR (400 MHz, $CDCl_3$) δ 7.57 – 7.49 (m, 6H), 7.43 (dd, J = 10.2, 4.7 Hz, 2H), 7.28 (d, J = 5.6 Hz, 1H), 6.73 (t, J = 5.6 Hz, 1H), 6.70 – 6.66 (m, 1H), 6.57 (s, 1H), 5.86 (s, 2H), 5.81 (s, 1H), 2.38 – 2.35 (m, 9H), 1.83 (s, 3H), 1.75 (d, J = 9.2 Hz, 6H).

ESI-MS (m/z): 628.1288, calcd. 628.1800 for $[M]^+$.

IR (KBr, cm^{-1}): 3068 (w), 2910 (w), 1606 (m), 1531 (m), 1484 (s), 1346 (m), 1272 (m), 1159 (w), 1024 (w), 971 (m), 777 (m), 671 (w).

Synthesis of In-4: $InMe_3$ (48.0 mg, 0.3 mmol) was slowly added to the solution of **HL4** (148.9 mg, 0.8 mmol) in toluene (5 mL). The reaction mixture was stirred for 2 hours at room temperature then heated to reflux overnight under nitrogen atmosphere to give a yellow solution. After cooling, toluene was removed in vacuo. The solid residue was washed three times with diethyl ether to remove any unreacted **HL4**. The crude product was redissolved in CH_2Cl_2 and filtered. Recrystallized by the addition of diethyl ether to give the desired product **In-4** as a yellow solid. Yield: 100.5 mg (50%).

^{1}H NMR (400 MHz, $CDCl_3$) δ 7.56 – 7.44 (m, 6H), 7.40 (d, J = 5.3 Hz, 1H), 7.34 – 7.27 (m, 2H), 6.72 – 6.47 (m, 3H), 2.28 (d, J = 4.1 Hz, 9H), 1.91 (dd, J = 17.5, 6.5 Hz, 9H), 1.72 (dd, J = 13.4, 8.0 Hz, 9H).

ESI-MS (m/z): 670.1716, calcd. 670.2270 for $[M]^+$.

IR (KBr, cm^{-1}): 2911 (m), 2854 (m), 1602 (s), 1473 (s), 1351 (s), 1251 (m), 1159 (m), 1006 (m), 939 (m), 773 (m), 669 (w).

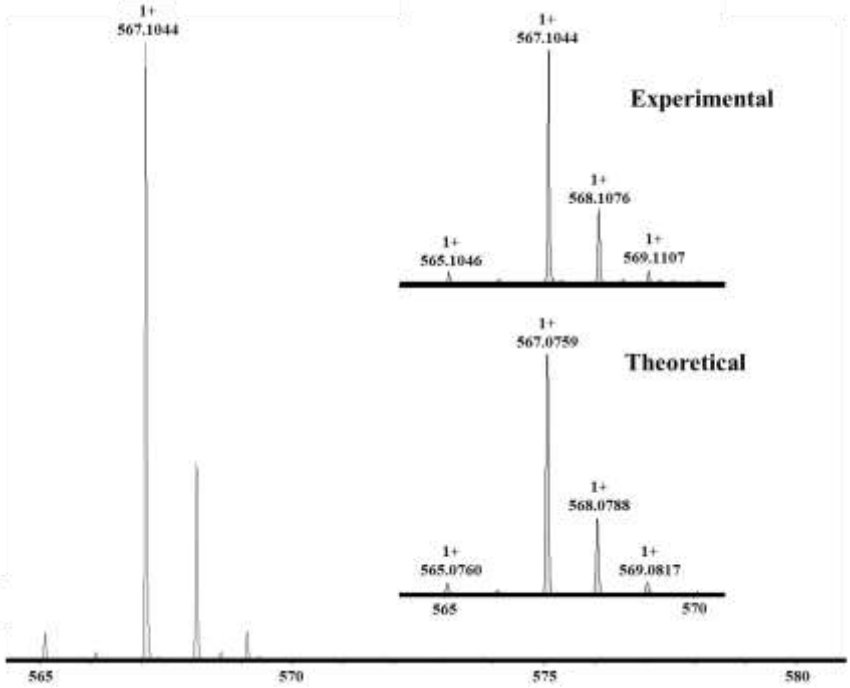

Figure S2. ESI-MS spectrum of complex **In-1** in CH_3CN. Inset: the comparison of observed and predicted isotope distribution.

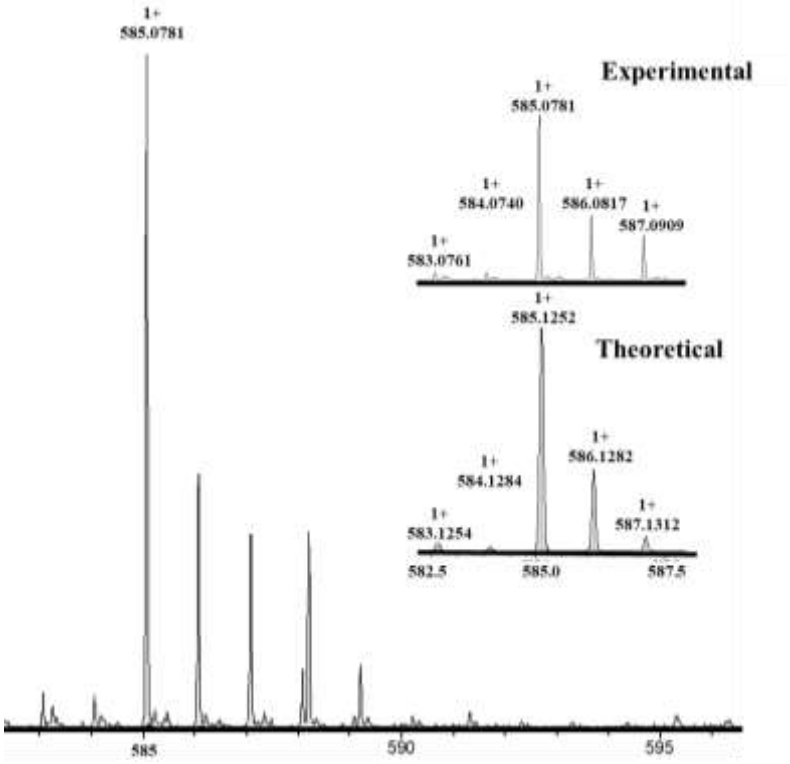

Figure S3. ESI-MS spectrum of complex **In-2** in CH_3CN. Inset: the comparison of observed and predicted isotope distribution.

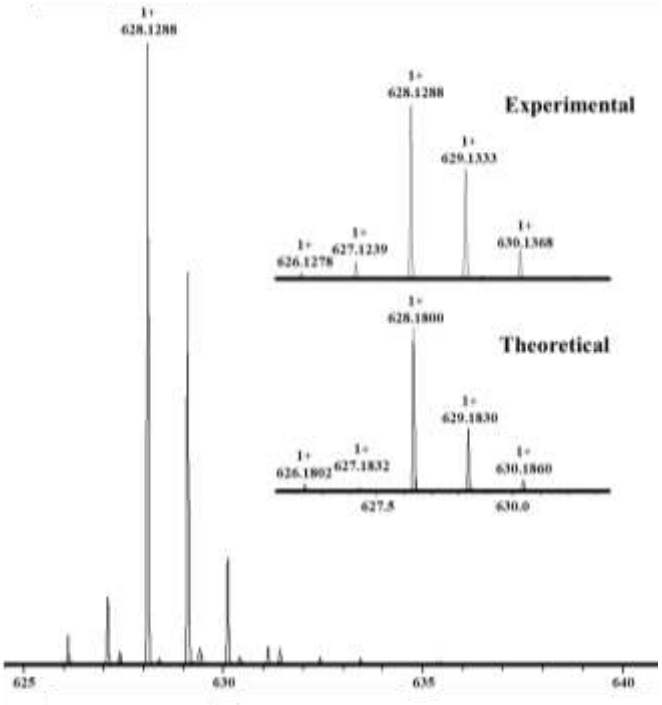

Figure S4. ESI-MS spectrum of complex **In-3** in CH_3CN. Inset: the comparison of observed and predicted isotope distribution.

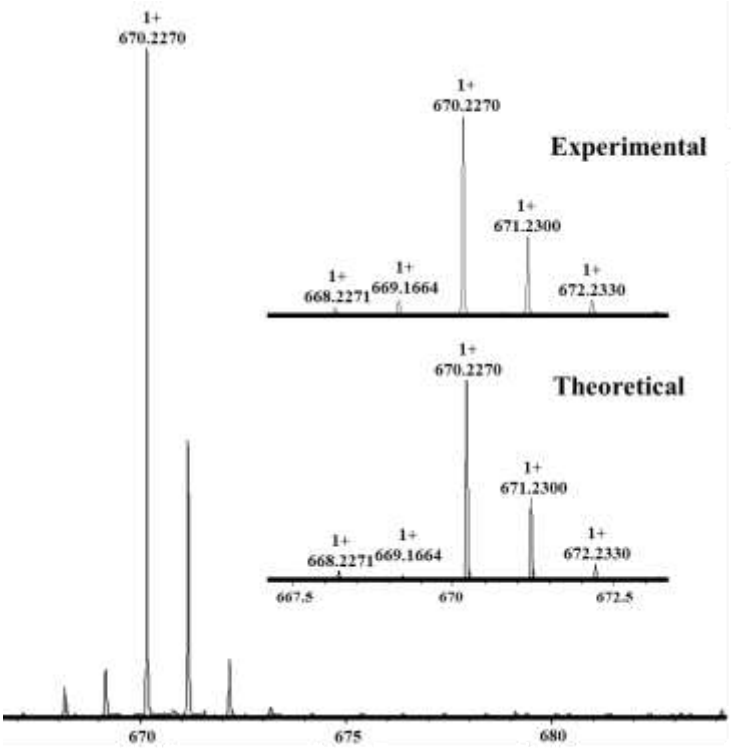

Figure S5. ESI-MS spectrum of complex **In-4** in CH_3CN. Inset: the comparison of observed and predicted isotope distribution.

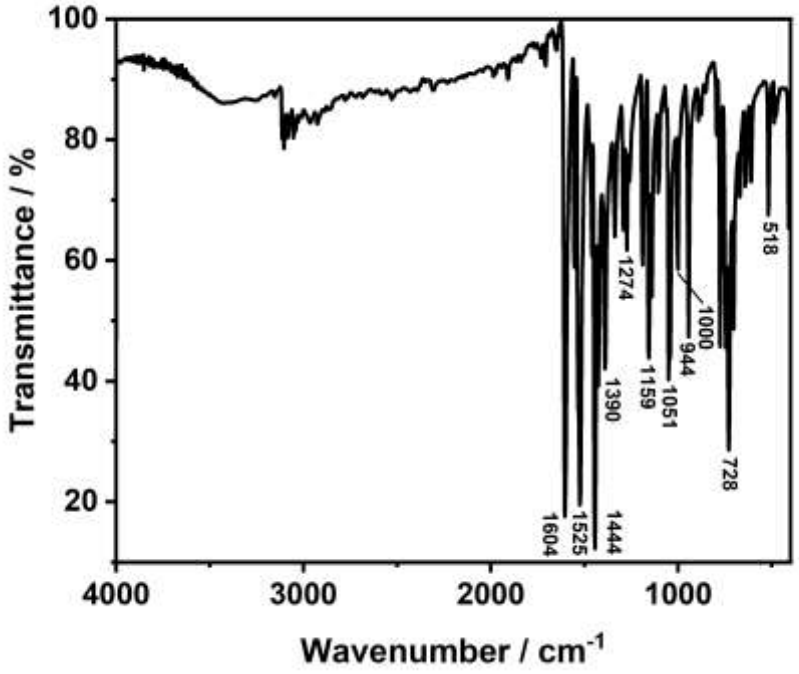

Figure S6. IR spectrum of complex **In-1**.

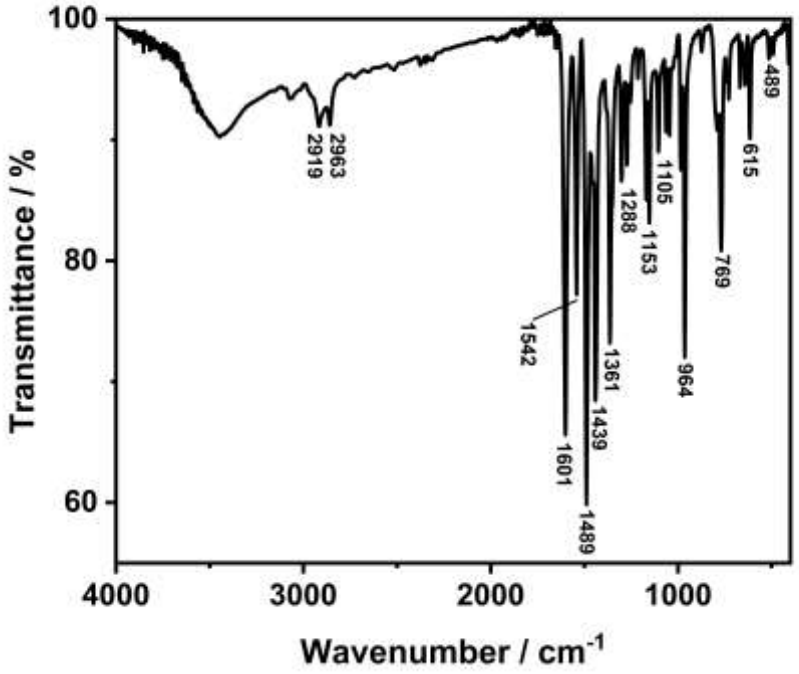

Figure S7. IR spectrum of complex **In-2**.

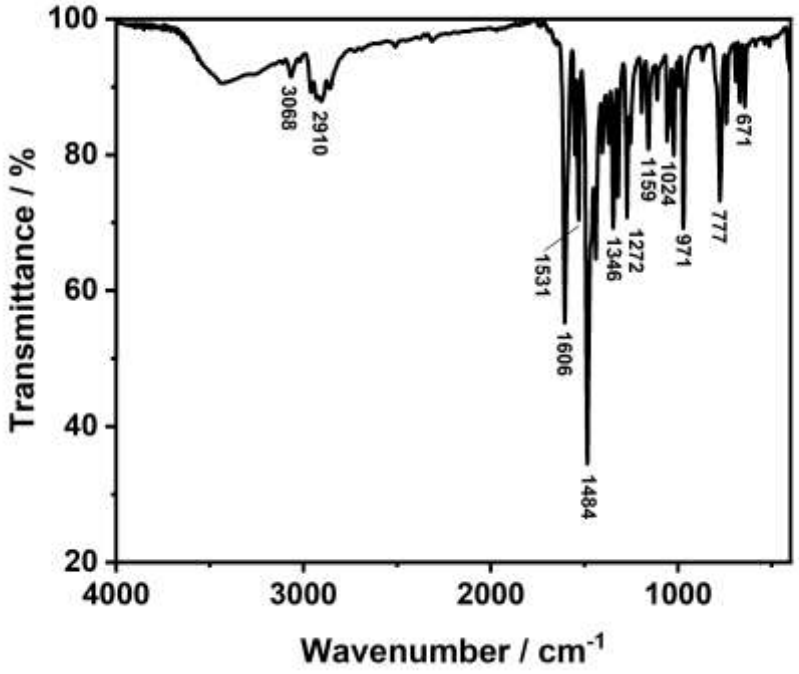

Figure S8. IR spectrum of complex **In-3**.

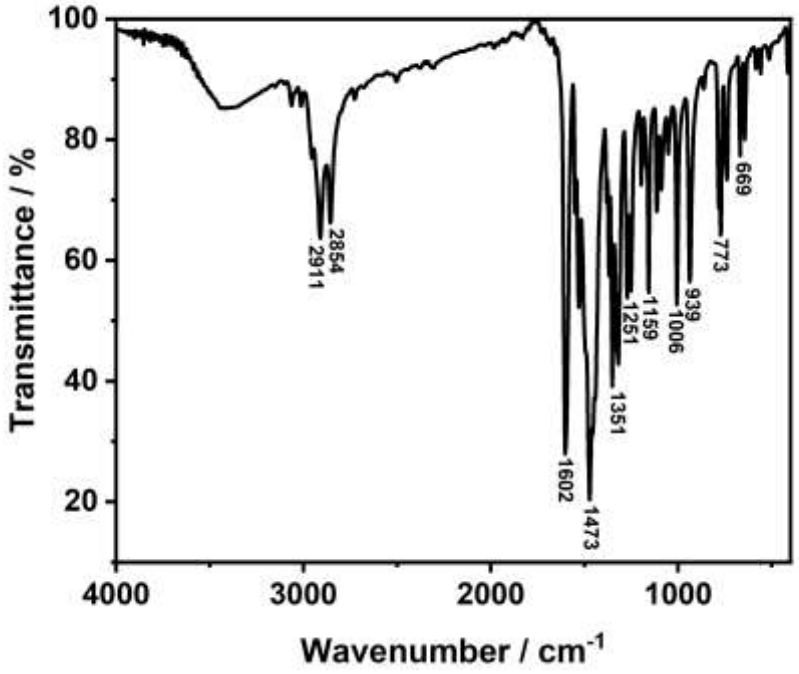

Figure S9. IR spectrum of complex **In-4**.

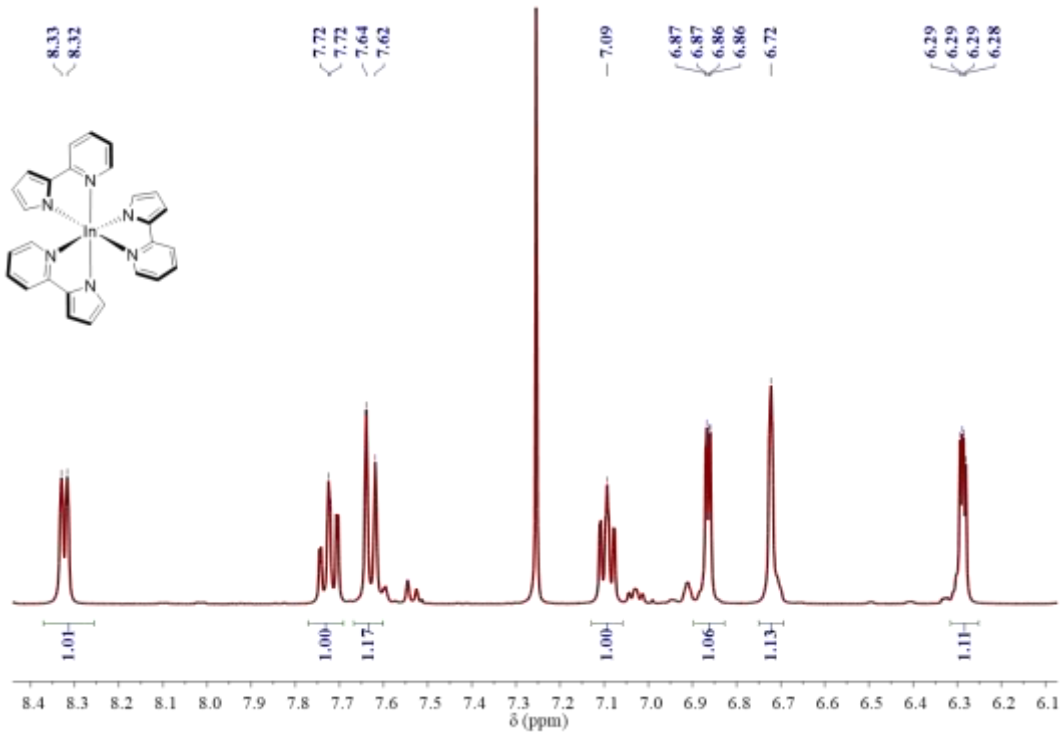

Figure S10. ^{1}H NMR spectrum of complex **In-1** in $CDCl_3$.

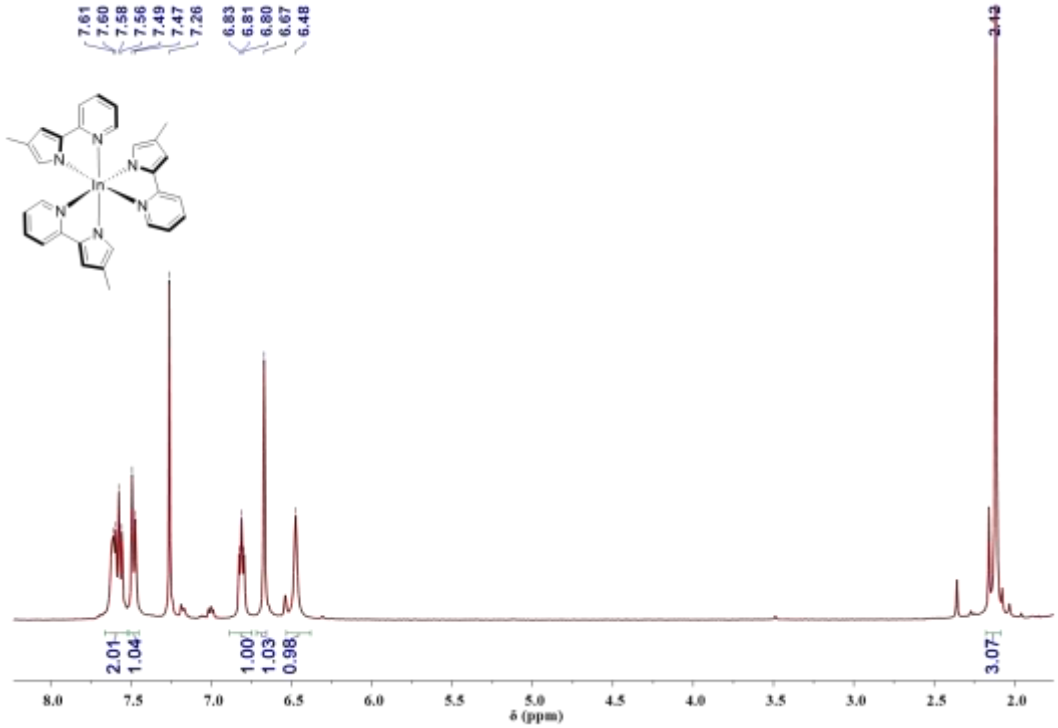

Figure S11. ^{1}H NMR spectrum of complex **In-2** in $CDCl_3$.

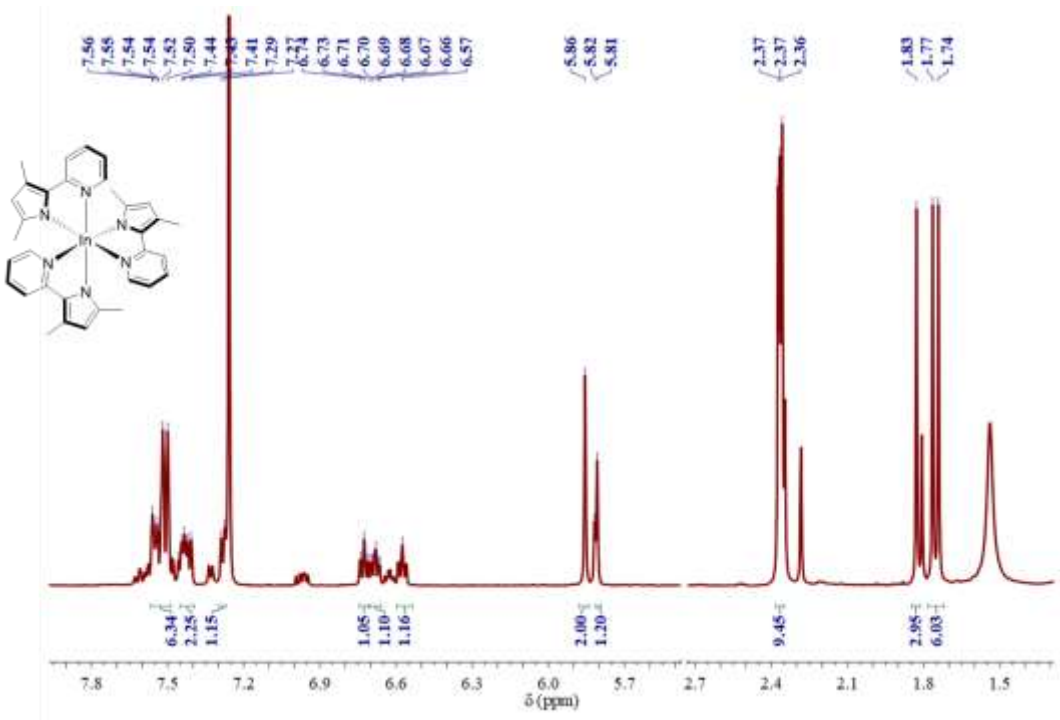

Figure S12. ^{1}H NMR spectrum of complex **In-3** in $CDCl_3$.

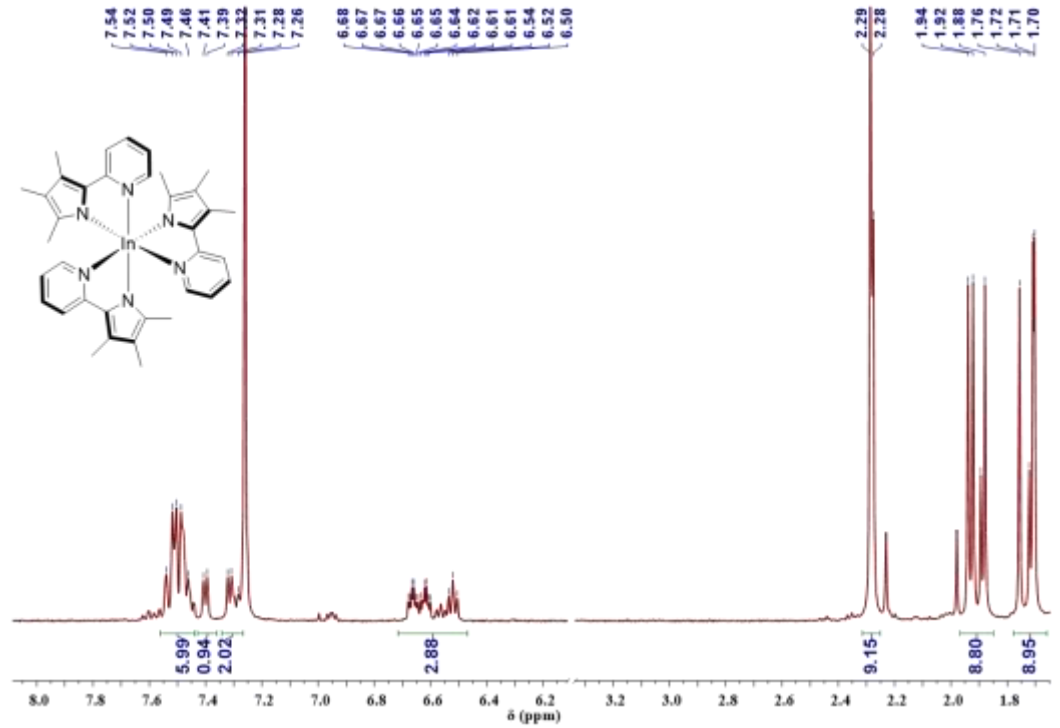

Figure S13. ^{1}H NMR spectrum of complex **In-4** in $CDCl_3$.

3. Crystallographic Data

Table S1. X-ray crystallographic data for complexes **In-1** and **In-3**.

Compound	**In-1**	**In-3**
Empirical formula	$C_{27}H_{21}InN_6$	$C_{33}H_{33}InN_6$
CCDC number	2257308	2257309
Formula weight	544.32	628.47
T/K	296(2)	296.15
Crystal system	monoclinic	triclinic
Space group	$P2_1/c$	P-1
a/Å	16.1797(10)	9.9431(2)
b/Å	15.4641(10)	10.4086(2)
c/Å	9.7077(6)	14.7800(3)
α/°	90	83.547(2)
β/°	99.032(3)	80.2990(10)
γ/°	90	74.8850(10)
V/Å^3	2398.8(3)	1451.83(5)
Z	4	2
ρ_{calc}/g·cm^{-3}	1.507	1.438
μ/mm^{-1}	1.012	0.847
F(000)	1096.0	644.0
Reflections collected	16047	18624
Independent reflections	5342 [R_{int} = 0.0204, R_{sigma} = 0.0280]	6583 [R_{int} = 0.0284, R_{sigma} = 0.0403]
Data/restraints/parameters	5342/102/286	6583/216/466
[a]Goodness-of-fit on F^2	1.061	1.045
[b]Final R indexes [I>=2σ (I)]	R_1 = 0.0950, wR_2 = 0.2616	R_1 = 0.0455, wR_2 = 0.1146
Final R indexes [all data]	R_1 = 0.1196, wR_2 = 0.2811	R_1 = 0.0634, wR_2 = 0.1232

[a]GoF = $[\Sigma w(|F_o| - |F_c|)^2/(N_{obs} - N_{param})]^{½}$.

[b]$R_1 = \Sigma||F_o| - |F_c||/\Sigma|F_o|$. [c]$wR_2$ $[(\Sigma w|F_o| - |F_c|)^2/\Sigma w^2|F_o|^2]^{½}$.

Table S2. Selected bond lengths (Å) and angles (˚)

Compound	**In-1**	**In-3**
	Bond lengths (Å)	
In1-N1	2.163(7)	2.200(3)
In1-N2	2.287(7)	2.278(4)
In1-N3	2.125(10)	2.186(4)
In1-N4	2.290(7)	2.223(4)
In1-N5	2.184(5)	2.211(3)
In1-N6	2.264(5)	2.327(4)
In1-N3’		2.211(7)
In1-N4’		2.282(6)
	Angles (˚)	
N1-In1-N2	75.1(3)	74.04(15)
N1-In1-N3	104.9(3)	96.8(2)
N1-In1-N6	157.0(3)	89.70(13)
N2-In1-N3	100.0(3)	103.95(18)
N2-In1-N6	90.3(3)	92.87(13)
N3-In1-N6	94.9(3)	163.06(17)
N4-In1-N1	99.5(3)	101.8(2)
N4-In1-N2	171.6(3)	175.67(19)
N4-In1-N3	74.8(3)	75.2(2)
N4-In1-N6	96.7(3)	88.19(18)
N5-In1-N1	90.6(3)	156.01(14)
N5-In1-N2	94.6(3)	89.16(14)
N5-In1-N3	160.9(3)	103.9(2)
N5-In1-N4	92.0(3)	95.16(19)
N5-In1-N6	72.6(3)	73.86(13)
N3’-In1-N1		103.6(2)
N3’-In1-N2		161.5(2)
N3’-In1-N5		97.7(2)
N3’-In1-N6		105.5(2)
N3’-In1-N4’		74.6(3)
N4’-In1-N1		94.4(2)
N4’-In1-N2		87.1(2)
N4’-In1-N5		101.8(2)
N4’-In1-N6		175.68(19)

4. DFT Calculation

DFT calculations were performed by using the Gaussian 09 package[4]. Geometry optimizations were performed on the ground state structures with the Becke's three-parameter B3LYP exchange-correlation functional[5,6]. The all-electron Gaussian basis sets were those developed by the Ahlrichs group[7-9]. The slightly smaller polarized split-valence def2-SVP basis sets for H, C, N and In atom Vibrational frequencies were calculated based on the optimized structures to confirm the absence of imaginary frequencies. MOs of complexes were calculated and visualized as well. The excited states calculations were carried out on the basis of the optimized S0 structures via time-dependent DFT (TD-DFT)[10] at the same level. The solvation effects were also taken into account using the self-consistent reaction field (SCRF) and a universal solvation model density (SMD)[11] with the acetonitrile solvent.

Input File Examples

Geometry Optimizations

```
%chk=In-1.chk

%mem=6GB

%nprocshared=8

#p b3lyp/def2SVP opt freq geom=connectivity



opt for In-1



0 1

Coordinates
```

TD-DFT Calculations

%chk=In-1-uv.chk

%mem=6GB

%nprocshared=8

#p td=(50-50, nstates=50, root=1) b3lyp/def2SVP SCRF(SMD,solvent=acetonitrile) geom=connectivity

uv for In-1

0 1

Coordinates

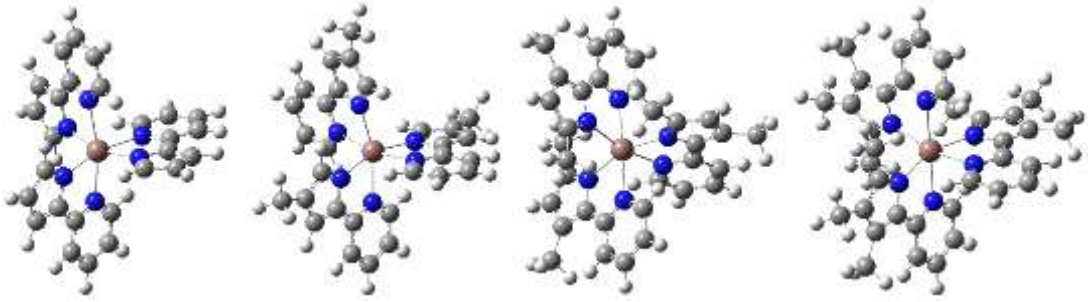

In-1 **In-2** **In-3** **In-4**

Figure S14. Optimized geometries for **In-1, In-2, In-3** and **In-4**

Table S3. Comparison of selected bond lengths (Å) and angles (°) of **In-1** and **In-3** from experimental and calculated results

Bond length/angle	**Calc. (In-1)**	**Exp. (In-1)**	**Calc. (In-3)**	**Exp. (In-3)**
In-N1	2.19939	2.163(7)	2.22226	2.200(3)
In-N2	2.34523	2.287(7)	2.33738	2.278(4)

In-N3	2.20332	2.125(10)	2.20492	2.186(4)
In-N4	2.34835	2.290(7)	2.34352	2.223(4)
In-N5	2.19892	2.184(5)	2.22436	2.211(3)
In-N6	2.38990	2.264(5)	2.35914	2.327(4)

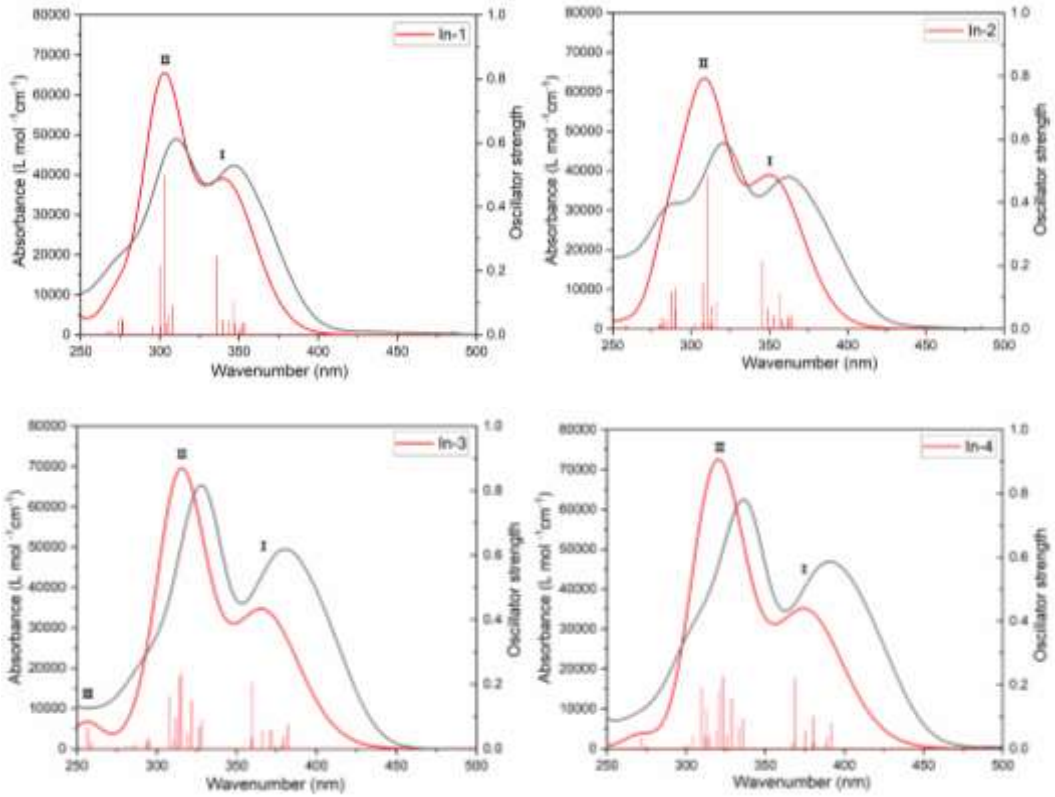

Figure S15. Electronic absorption spectrum of **In-1**, **In-2**, **In-3** and **In-4** obtained via TD-DFT calculations (red line, fwhm of 0.5 eV). The stick plot indicates the positions and relative intensities of individual transitions. Transitions with calculated oscillator strengths larger than 0.03 are labeled according to their TD-DFT state number. The experimental spectrum is shown as a black line for comparison.

Table S4. Vertical Electronic Excitation Energies and Main Excitations Contributing to the Absorption Bands of **In-1**, **In-2**, **In-3** and **In-4** Obtained via TD-DFT Calculations.

	band	state	E (eV)	λ (nm)	f_{osc}	Excitations (weight)[a,b]	Character
In-1	**I**	16	3.5763	346.68	0.1077	122→125 (0.64)	^{1}LLCT
						123→125 (0.08)	^{1}LLCT + ^{1}ILCT
		21	3.6885	336.14	0.2446	121→126 (0.74)	^{1}LLCT + ^{1}ILCT
	II	32	4.0952	302.76	0.4962	121→128 (0.27)	^{1}LLCT
						122→127 (0.20)	^{1}LLCT + ^{1}ILCT
						122→128 (0.23)	^{1}LLCT
		35	4.1333	299.97	0.2183	123→129 (0.56)	^{1}LLCT + ^{1}ILCT
						121→129 (0.13)	^{1}LLCT
In-2	**I**	16	3.4743	356.86	0.1127	134→137 (0.57)	^{1}LLCT + ^{1}ILCT
						133→138 (0.08)	^{1}LLCT + ^{1}ILCT
						134→136 (0.05)	^{1}LLCT + ^{1}ILCT
		19	3.5485	349.40	0.0646	134→138 (0.59)	^{1}LLCT + ^{1}ILCT
		21	3.5853	345.81	0.2163	133→138 (0.79)	^{1}LLCT + ^{1}ILCT
	II	25	3.9192	316.35	0.0875	135→139 (0.85)	^{1}LLCT + ^{1}ILCT
		31	3.9890	310.82	0.4836	134→140 (0.27)	^{1}LLCT + ^{1}ILCT
						134→139 (0.20)	^{1}LLCT + ^{1}ILCT

						133→140 (0.15)	^{1}ILCT
		35	4.0307	307.60	0.1446	135→141 (0.52)	^{1}LLCT + ^{1}ILCT
						134→140 (0.10)	^{1}LLCT + ^{1}ILCT
						134→141 (0.08)	^{1}LLCT + ^{1}ILCT
In-3	**I**	7	3.2414	382.51	0.0761	147→148 (0.88)	^{1}LLCT + ^{1}ILCT
						145→148 (0.05)	^{1}LLCT + ^{1}ILCT
		15	3.3356	371.69	0.0582	146→149 (0.00)	^{1}LLCT + ^{1}ILCT
		16	3.3443	370.73	0.0577	145→149 (0.62)	^{1}LLCT + ^{1}ILCT
		18	3.3850	366.27	0.0561	147→150 (0.64)	^{1}LLCT + ^{1}ILCT
						146→150 (0.19)	^{1}LLCT + ^{1}ILCT
						145→149 (0.07)	^{1}LLCT + ^{1}ILCT
		20	3.4438	360.02	0.2040	146→150 (0.66)	^{1}LLCT + ^{1}ILCT
	II	29	3.8479	322.21	0.1492	145→151 (0.41)	^{1}LLCT + ^{1}ILCT
						146→152 (0.35)	^{1}LLCT + ^{1}ILCT
		33	3.9283	315.62	0.2348	146→152 (0.41)	^{1}LLCT + ^{1}ILCT
						147→153 (0.10)	^{1}LLCT + ^{1}ILCT
						147→152 (0.08)	^{1}LLCT + ^{1}ILCT

						145→153 (0.08)	^{1}LLCT + ^{1}ILCT
		34	3.9453	314.26	0.2250	147→153 (0.67)	^{1}LLCT + ^{1}ILCT
		35	3.9700	312.31	0.0969	145→152 (0.51)	^{1}LLCT + ^{1}ILCT
						146→152 (0.19)	^{1}LLCT + ^{1}ILCT
						145→153 (0.09)	^{1}LLCT + ^{1}ILCT
		39	4.0240	308.11	0.1632	145→153 (0.57)	^{1}LLCT + ^{1}ILCT
						146→153 (0.26)	^{1}LLCT + ^{1}ILCT
In-4	**I**	7	3.1621	392.10	0.0787	159→160 (0.89)	^{1}LLCT + ^{1}ILCT
		16	3.2623	380.06	0.1015	157→161 (0.69)	^{1}LLCT + ^{1}ILCT
						159→162 (0.09)	^{1}LLCT + ^{1}ILCT
						159→161 (0.07)	^{1}LLCT + ^{1}ILCT
		18	3.3050	375.14	0.0562	159→162 (0.70)	^{1}LLCT + ^{1}ILCT
						158→162 (0.13)	^{1}LLCT + ^{1}ILCT
		20	3.3650	368.45	0.2200	158→162 (0.64)	^{1}LLCT + ^{1}ILCT
						157→162 (0.15)	^{1}LLCT + ^{1}ILCT
	II	29	3.7691	328.95	0.1567	157→163 (0.58)	^{1}LLCT + ^{1}ILCT
						159→163 (0.08)	^{1}LLCT +

					^{1}ILCT
32	3.8385	323.00	0.2262	158→164 (0.48)	^{1}LLCT + ^{1}ILCT
				159→164 (0.11)	^{1}LLCT + ^{1}ILCT
				157→164 (0.07)	^{1}LLCT + ^{1}ILCT
				158→165 (0.06)	^{1}LLCT + ^{1}ILCT
34	3.8607	321.14	0.1804	159→165 (0.63)	^{1}LLCT + ^{1}ILCT
				155→160 (0.06)	^{1}LLCT + ^{1}ILCT
40	3.9667	312.57	0.1246	156→160 (0.67)	^{1}LLCT + ^{1}ILCT
				158→164 (0.15)	^{1}LLCT + ^{1}ILCT
42	4.0016	309.84	0.1916	155→160 (0.32)	^{1}LLCT + ^{1}ILCT
				156→161 (0.28)	^{1}LLCT + ^{1}ILCT
				157→165 (0.22)	^{1}LLCT + ^{1}ILCT

[a] Only excitations contribution with a weight larger than 0.05 are shown. [b] for **In-1**: HOMO 123, LUMO 124; **In-2**: HOMO 135, LUMO 136; **In-3**: HOMO 147, LUMO 148; **In-4**: HOMO 159, LUMO 160.

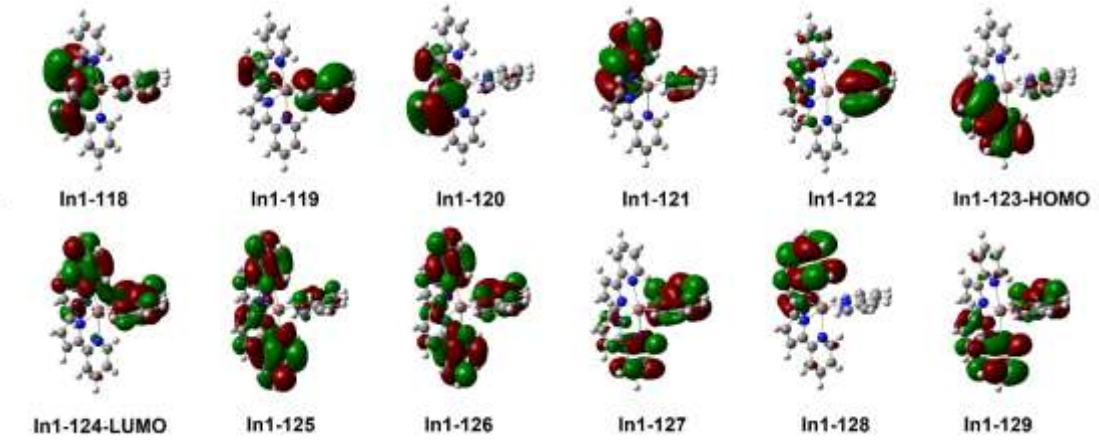
In1-118
In1-119
In1-120
In1-121
In1-122
In1-123-HOMO
In1-124-LUMO
In1-125
In1-126
In1-127
In1-128
In1-129

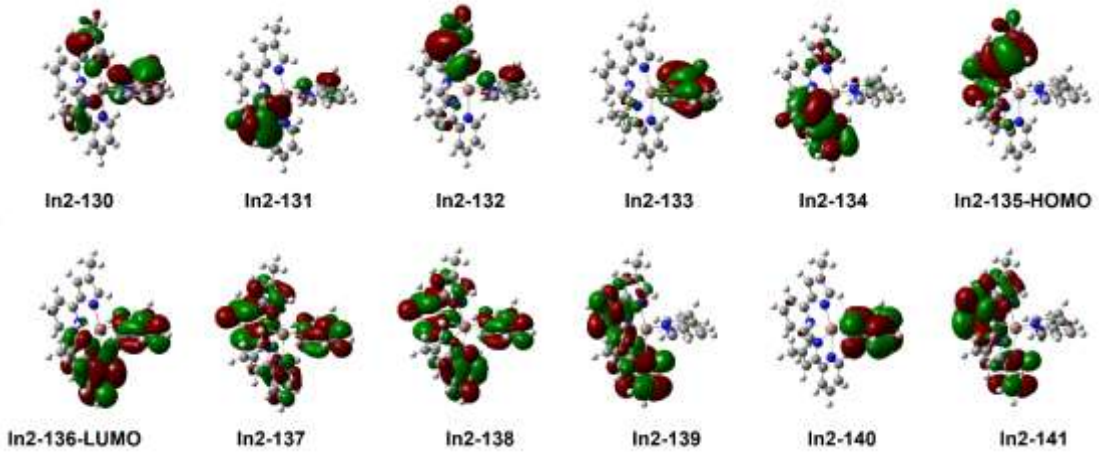
In2-130
In2-131
In2-132
In2-133
In2-134
In2-135-HOMO
In2-136-LUMO
In2-137
In2-138
In2-139
In2-140
In2-141

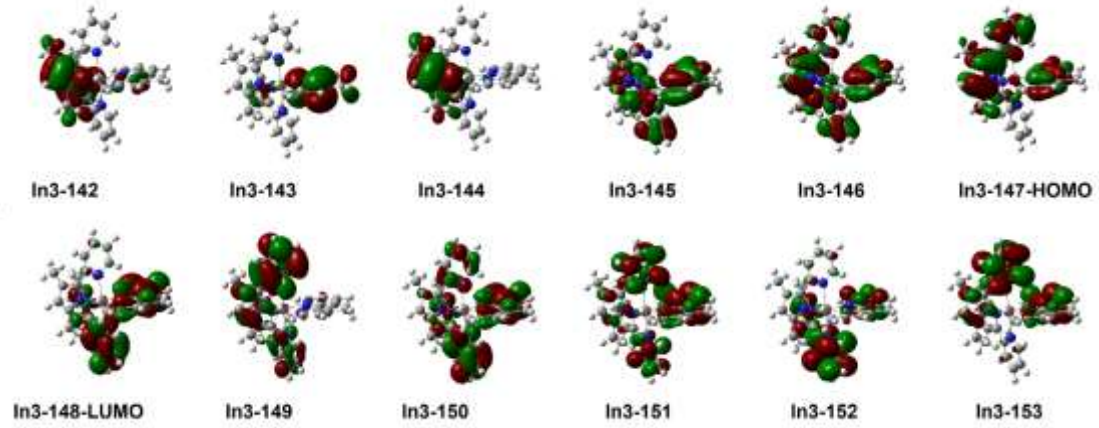
In3-142
In3-143
In3-144
In3-145
In3-146
In3-147-HOMO
In3-148-LUMO
In3-149
In3-150
In3-151
In3-152
In3-153

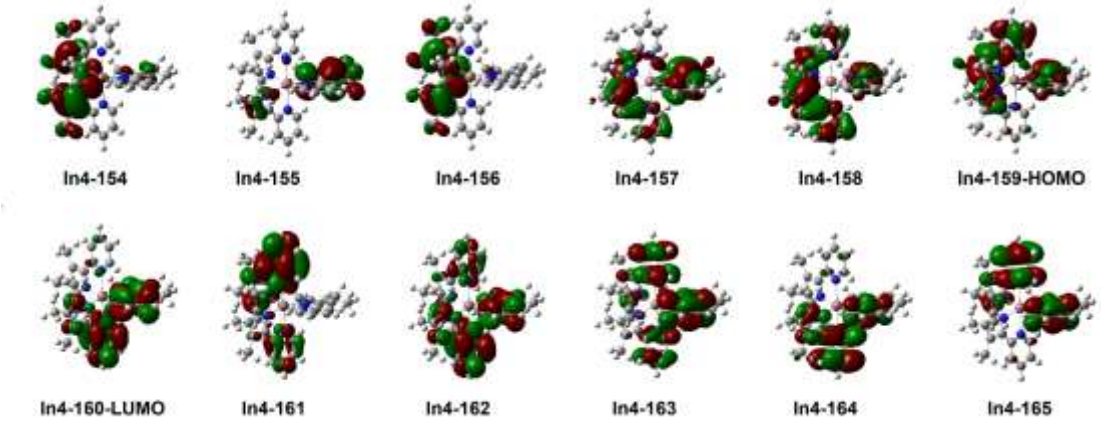

Figure S16. Frontier molecular orbital diagram of **In-1, In-2, In-3** and **In-4** showing the donor and acceptor orbitals contributing to TD-DFT excitations computed in visible region of electronic absorption spectrum.

5. Absorption and Emission Spectra in Various Solvents

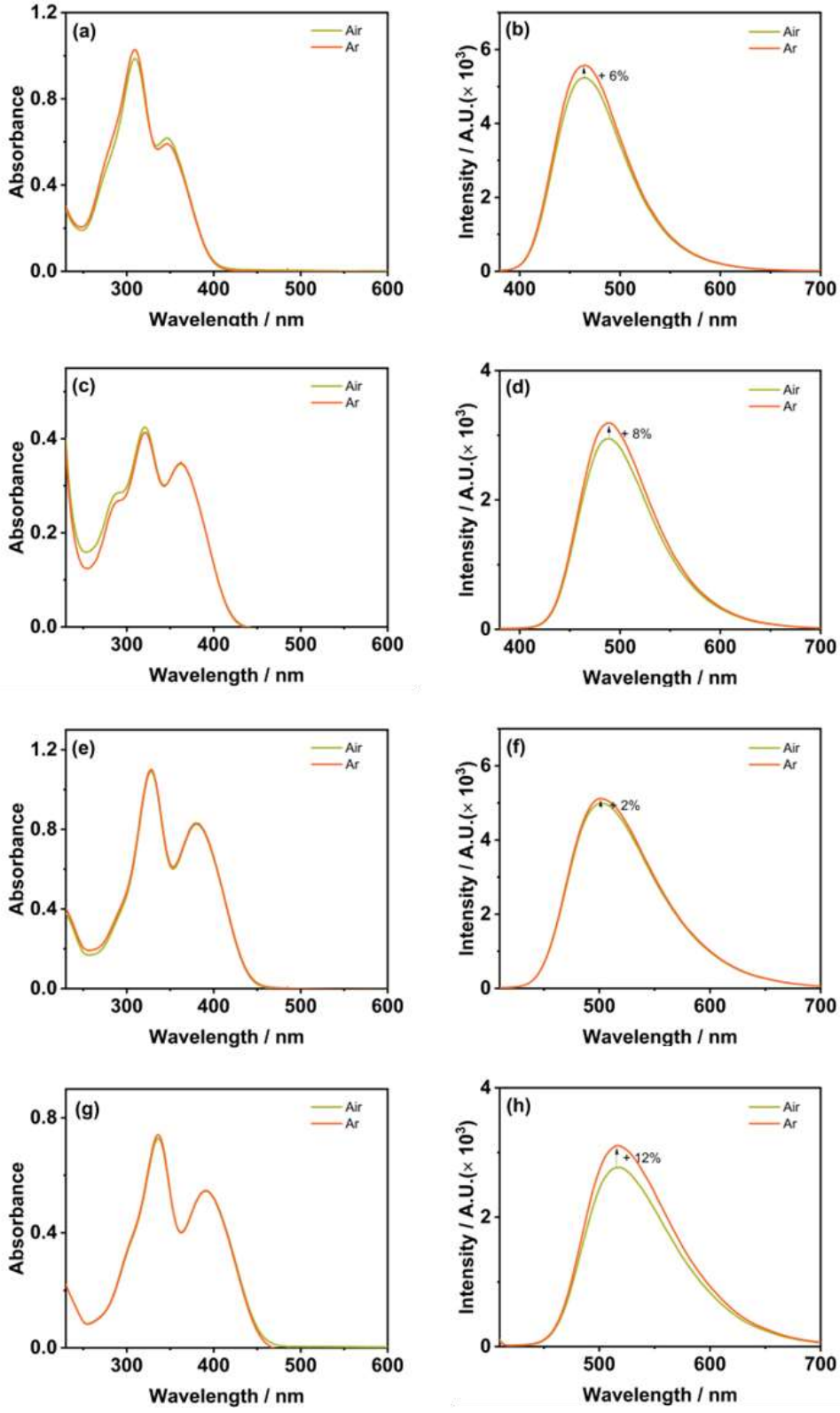

Figure S17. The absorption spectra (a) and emission spectra (b) of **In-1** in CH_3CN solution under argon atmosphere or upon exposure to air; The absorption spectra (c)

and emission spectra (d) of **In-2** in CH_3CN solution under argon atmosphere or upon exposure to air; The absorption spectra (e) and emission spectra (f) of **In-3** in CH_3CN solution under argon atmosphere or upon exposure to air; The absorption spectra (g) and emission spectra (h) of **In-4** in CH_3CN solution under argon atmosphere or upon exposure to air.

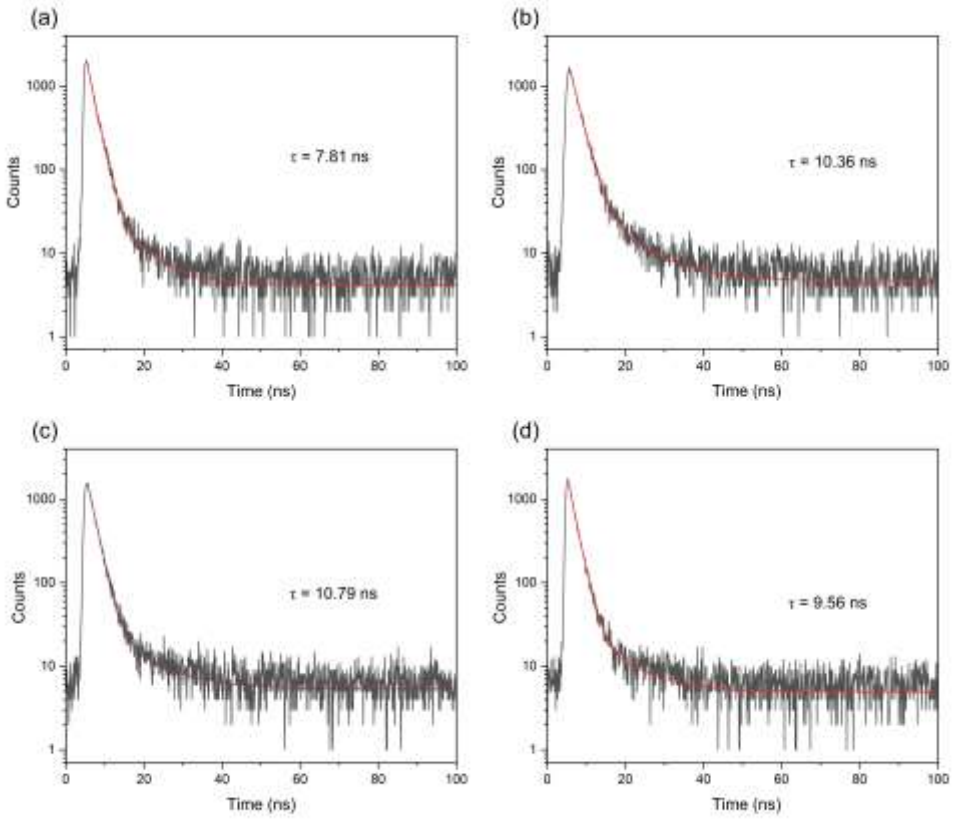

Figure S18. The excited state lifetimes of **In-1** (a), **In-2** (b), **In-3** (c) and **In-4** (d) in CH_3CN measured by time-resolved fluorescence spectroscopy in N_2 atmosphere.

6. Cyclic Voltammetry

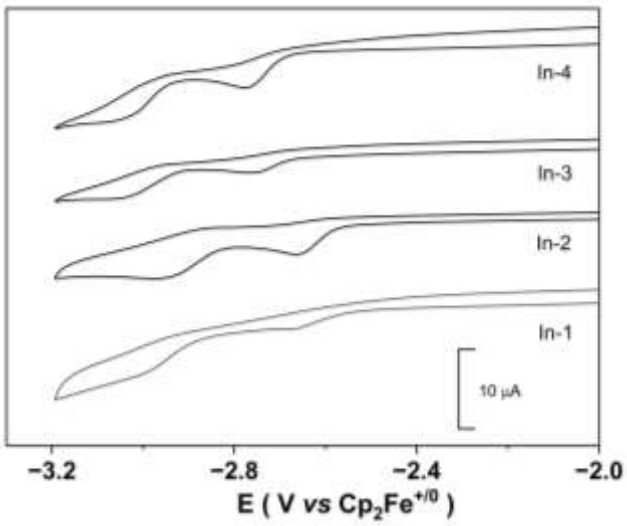

Figure S19. Reductive cyclic voltammetry of 0.1mM **In-1** - **In-4**, in degassed CH_3CN solution with scan rate at 0.1 V s^{-1}, electrolyte: 0.1 M Bu_4NPF_6, reference electrode: AgCl/Ag electrode in saturated KCl solution; counter electrode: Pt wire; working electrode: glassy carbon electrode, E vs. $Cp_2Fe^{+/0}$.

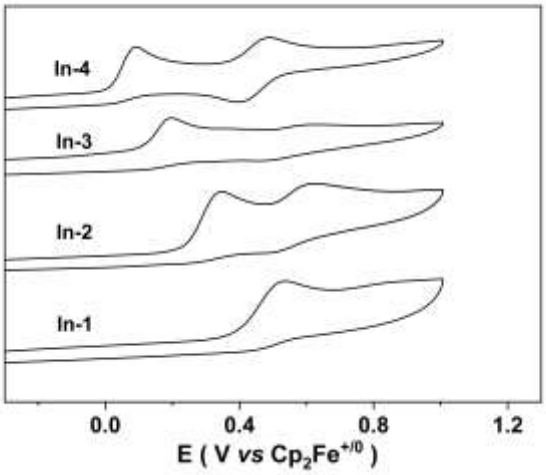

Figure S20. Oxidative cyclic voltammetry of 0.1mM **In-1** - **In-4**, in degassed CH_3CN solution with scan rate at 0.1 V s^{-1}, electrolyte: 0.1 M Bu_4NPF_6, reference electrode: AgCl/Ag electrode in saturated KCl solution; counter electrode: Pt wire; working electrode: glassy carbon electrode, E vs. $Cp_2Fe^{+/0}$.

7. Photoredox Catalysis

7.1 Experimental setup for photoredox reactions

All photoredox experiments were performed using Perfect Light PCX50C photochemistry system. Constant room temperature conditions were maintained using a water bath in a jacketed glass beaker with water cooling.

Figure S21. Experimental setup for irradiation of NMR tubes.

7.2 Indium(III) photosensitizers for photo-dehalogenation

The NMR tube was charged with photosensitizer (0.001 mmol, 1.0 equiv.), BIH (13.3 mg, 0.059 mmol, 59.0 equiv,), and ethyl bromodifluoroacetate (12.0 mg, 0.059 mmol, 59.0 equiv,) and C_6D_6 (0.6 mL) in the dry-box. The mixture was placed in a jacketed glass beaker with water cooling (at r. t.) and irradiated with different light source for given time. 1,3,5-trimethoxybenzene as an internal standard was added into the reaction mixture, the yield was calculated by NMR spectroscopy.

Table S5. Condition optimization of photo-dehalogenation by indium(III) photosensitizers.

Entry	Complex	λ (nm)	Yield [a]
1	**In-1**	420	46
2	**In-1**	450	50
3	**In-1**	White light	33
4	**In-2**	420	15
5	**In-2**	450	9
6	**In-2**	White light	7
7	**In-3**	420	18
8	**In-3**	450	46
9	**In-3**	White light	7
10	**In-4**	420	24
11	**In-4**	450	35
12	**In-4**	White light	12
13	**In-1**	-	Trace
14	**In-2**	-	Trace
15	**In-3**	-	Trace
16	**In-4**	-	Trace
17	-	420	10
18	-	450	9
19	-	White light	8

[a] The yield was calculated by using 1,3,5-trimethoxybenzene as the internal standard, reaction time: 1 h.

a)

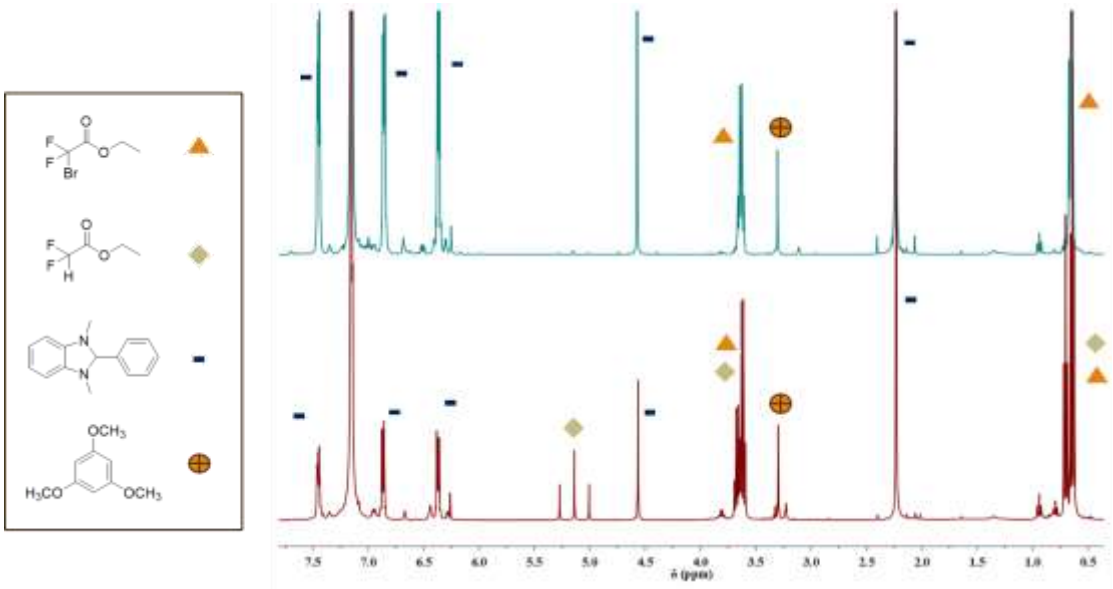

b)

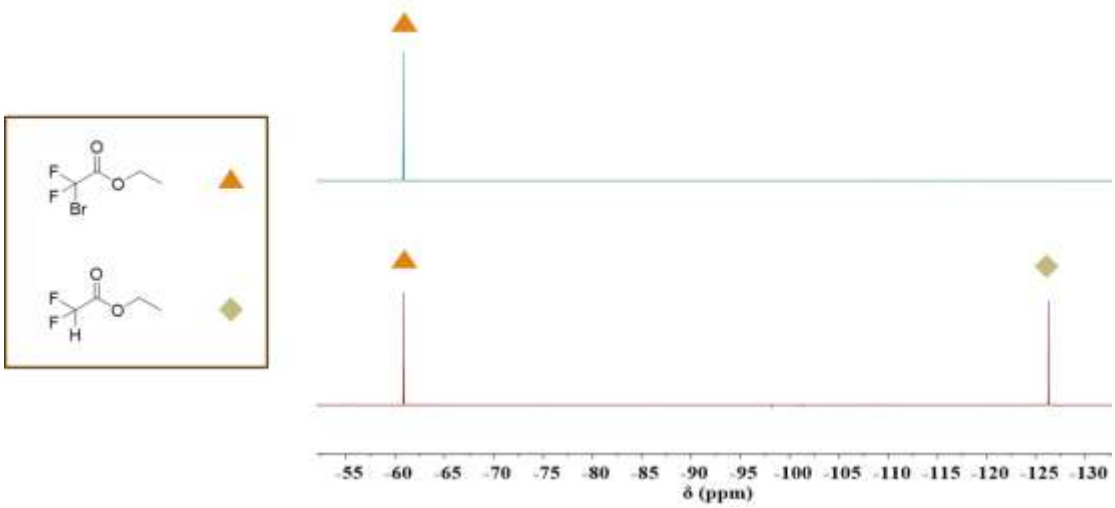

Figure S22. a) ^{1}H NMR spectra and b) ^{19}F NMR spectra of reaction mixture of ethyl bromodifluoroacetate and BIH in presence of catalyst **In-1** and internal standard 1,3,5-trimethoxybenzene before and after irradiation of 450 nm in C_6D_6.
grayish green line: ethyl bromodifluoroacetate + BIH + internal standard + **In-1**, 0 h;
brown line: ethyl bromodifluoroacetate + BIH + internal standard + **In-1**, 1 h;

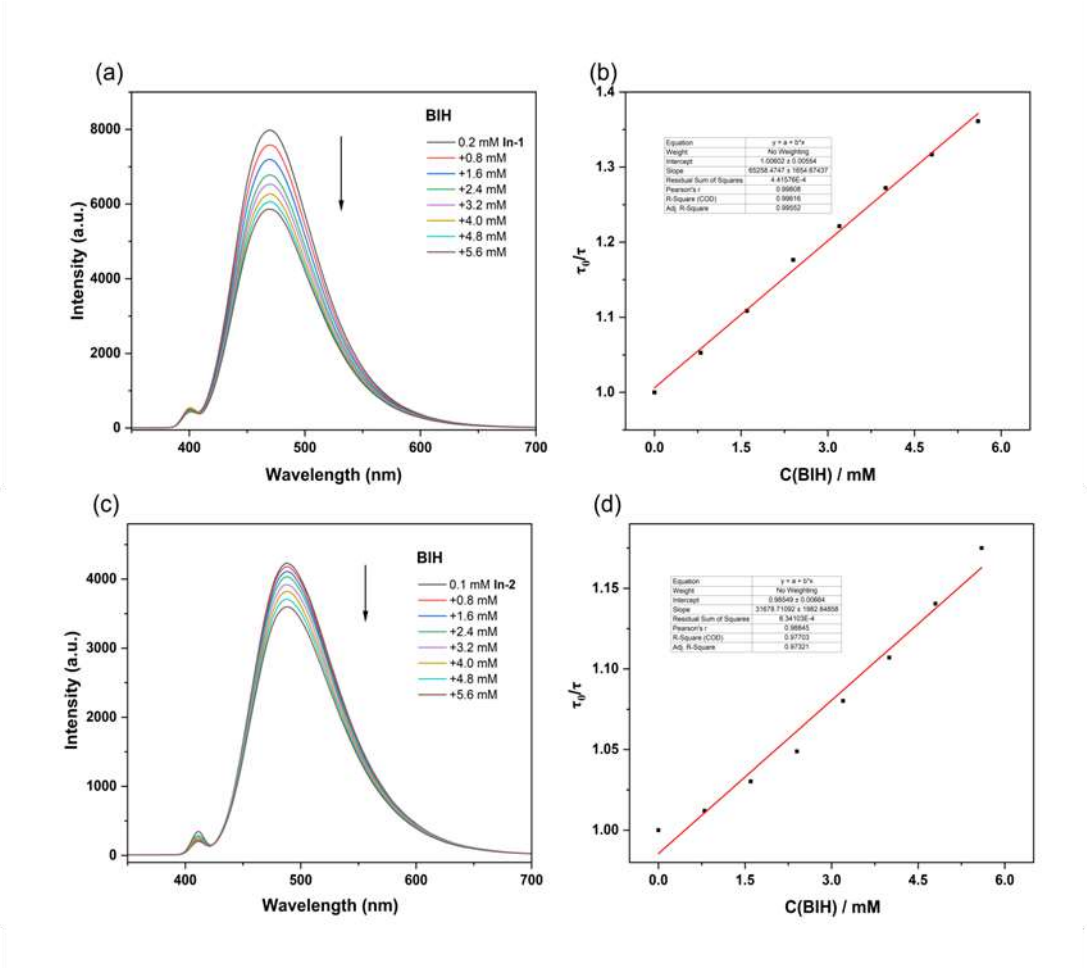

Figure S23. The fluorescence quenching curves of (a) **In-1**, (c) **In-2** with BIH. (b)(d) BIH on **In-1** and **In-2** Stern-Volmer quenching curve. K_q(**In-1**)=8.37×10^9 $M^{-1}S^{-1}$;K_q(**In-2**)=3.05×10^9 $M^{-1}S^{-1}$

7.3 Indium(III) photosensitizers for reduction of cis-diethyl maleate

The NMR tube was charged with photosensitizers (1 mg, 0.001 mmol, 1.0 equiv.), BIH (10.8 mg, 0.048 mmol, 48.0 equiv,), and cis-diethyl maleate (4.1 mg, 0.024 mmol, 24.0 equiv,) and 0.6 mL C_6D_6 in the dry-box. The mixture was placed in a water-cooled glass vessel and irradiated with different irradiation. 1,3,5-trimethoxybenzene was added as an internal standard. The products were analyzed by ^{1}H NMR spectroscopy and the yields are based on internal standard. The ^{1}H NMR spectroscopic data of diethyl maleate, diethyl fumarate, and diethyl succinate in C_6D_6 and $CDCl_3$ were established from commercially available pure materials.

Table S6. Reduction of cis-diethyl maleate using indium(III) photosensitizers.

Entry	Complex	λ (nm)	Yield (a/b) [a]
1	**In-1**	450	38:22
2	**In-2**	450	40:60
3	**In-3**	450	73:26
4	**In-4**	450	61:39
5	**In-1**	-	Trace
6	**In-2**	-	Trace
7	**In-3**	-	Trace
8	**In-4**	-	Trace
9	-	450	Trace

[a] The yield was calculated by using 1,3,5-trimethoxybenzene as the internal standard. The reaction time: 2 h.

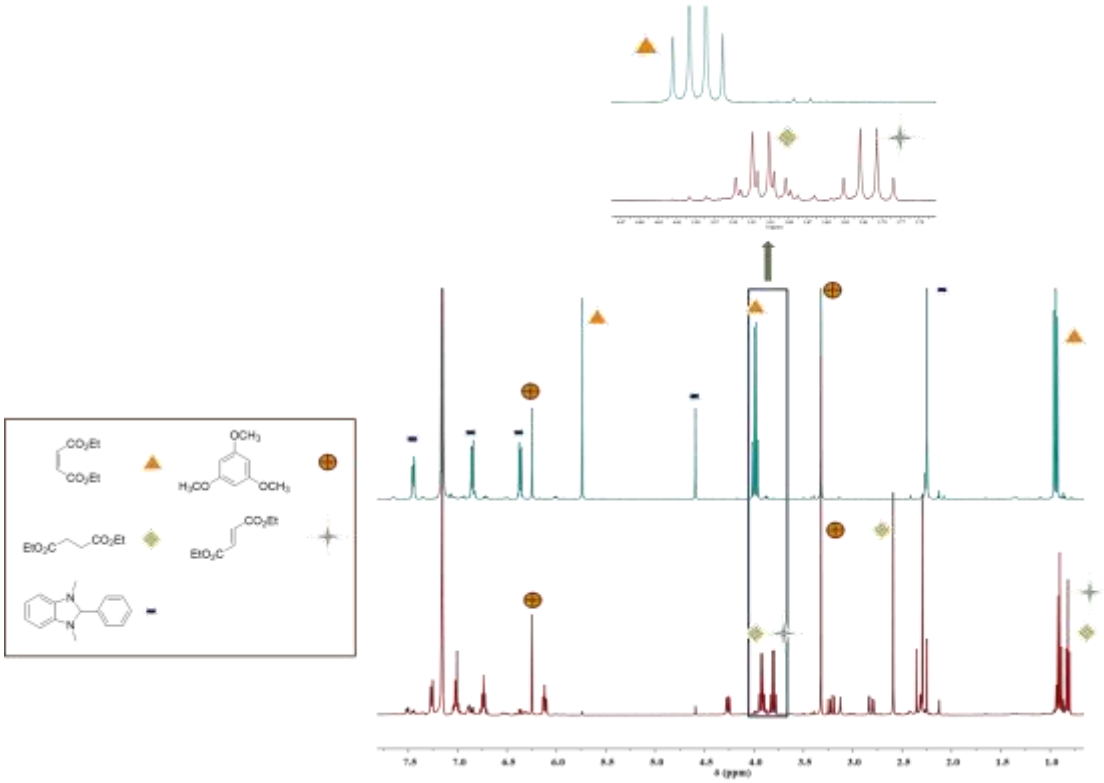

Figure S24. ^{1}H NMR spectra of reaction mixture of diethyl maleate, BIH and in presence of catalyst **In-2** and internal standard 1,3,5-trimethoxybenzene before and after irradiation of 450 nm in C_6D_6.
grayish green line: diethyl maleate + BIH + internal standard + **In-2**, 0 h;
brown line: diethyl maleate + BIH + internal standard + **In-2**, 2 h.

8. References

1. Ducloiset, C.; Jouin, P.; Paredes, E.; Guillot, R.; Sircoglou, M.; Orio, M.; Leibl, W.; Aukauloo, A. Monoanionic dipyrrin–pyridine ligands: synthesis, structure and photophysical properties. *Eur. J. Inorg. Chem.*, **2015**, 32, 5405-5410.
2. Klappa, J. J.; Rich, A. E.; McNeill, K. One-step synthesis of 3, 5-disubstituted-2-pyridylpyrroles from the condensation of 1, 3-diones and 2-(aminomethyl) pyridine. *Org. Lett.*, **2002**, 4, 435-437.
3. Reichardt, C. Empirical parameters of solvent polarity as linear free-energy relationships. *Angew. Chem. Int. Ed.*, **1979**, 18, 98-110.
4. Frisch, M. J., Trucks, G. W., Schlegel, H. B., Scuseria, G. E., Robb, M. A., Cheeseman, J. R., Scalmani, G., Barone, V., Mennucci, B., Petersson, G. A., Nakatsuji, H., Caricato, M., Li, X., Hratchian, H. P., Izmaylov, A. F., Bloino, J., Zheng, G., Sonnenberg, J. L., Hada, M., Ehara, M., Toyota, K., Fukuda, R., Hasegawa, J., Ishida, M., Nakajima, T., Honda, Y., Kitao, O., Nakai, H., Vreven, T., Montgomery, J. A., Jr., Peralta, J. E., Ogliaro, F., Bearpark, M., Heyd, J. J., Brothers, E., Kudin, K. N., Staroverov, V. N., Keith, T., Kobayashi, R., Normand, J., Raghavachari, K., Rendell, A., Burant, J. C., Iyengar, S. S., Tomasi, J., Cossi, M., Rega, N., Millam, N. J., Klene, M., Knox, J. E., Cross, J. B., Bakken, V., Adamo, C., Jaramillo, J., Gomperts, R., Stratmann, R. E., Yazyev, O., Austin, A. J., Cammi, R., Pomelli, C., Ochterski, J. W., Martin, R. L., Morokuma, K., Zakrzewski, V. G., Voth, G. A., Salvador, P., Dannenberg, J. J., Dapprich, S., Daniels, A. D., Farkas, O., Foresman, J. B., Ortiz, J. V., Cioslowski, J. & Fox, D. J. *Gaussian 09, Revision D.01*; Gaussian, Inc.: Wallingford CT, 2009.
5. Becke, A. D., *J. Chem. Phys.*, **1993**, 98 (7), 5648-5652.
6. Lee, C., Yang, W. and Parr, R. G., *Phys. Rev. B*, **1988**, 37 (2), 785-789.
7. Schäfer, A., Horn, H. and Ahlrichs, R., *J. Chem. Phys.*, **1992**, 97, 2571.
8. Schäfer, A., Huber, C. and Ahlrichs, R., *J. Chem. Phys.*, **1994**, 100, 5829.
9. Weigend. F. and Ahlrichs R., *Phys. Chem. Chem. Phys.*, **2005**, 7, 3297.
10. Fantacci, S., De Angelis, F. and Selloni, A., *J. Am. Chem. Soc.*, **2003**, 125 (14), 4381-4387.
11. Marenich A. V., Cramer C. J., and Truhlar D. G. *J. Phys. Chem. B*, **2009**, 113, 6378-6396.